0888-8809/06/$15.00/0
Printed in U.S.A.

Molecular Endocrinology 20(4):831–843

doi: 10.1210/me.2005-0384

Sequence-Specific Deoxyribonucleic Acid (DNA) Recognition by Steroidogenic Factor 1: A Helix at the Carboxy Terminus of the DNA Binding Domain Is Necessary for Complex Stability

Tanya H. Little, Yongbo Zhang, Christina K. Matulis, Jennifer Weck, Zhipeng Zhang, Aparna Ramachandran, Kelly E. Mayo, and Ishwar Radhakrishnan

Department of Biochemistry (T.H.L., Y.Z., C.K.M., J.W., Z.Z., A.R., K.E.M., I.R.), Molecular Biology, and Cell Biology, Northwestern University, Evanston, Illinois 60208-3500; Weinberg College of Arts and Sciences Structural Biology Nuclear Magnetic Resonance Facility (Y.Z.), Northwestern University, Evanston, Illinois 60208-3500; and Center for Reproductive Science (K.E.M.), Northwestern University, Evanston, Illinois 60208-3500

Steroidogenic factor 1 (SF1) is a member of the NR5A subfamily of nuclear hormone receptors and is considered a master regulator of reproduction because it regulates a number of genes encoding reproductive hormones and enzymes involved in steroid hormone biosynthesis. Like other NR5A members, SF1 harbors a highly conserved approximately 30-residue segment called the FTZ-F1 box C-terminal to the core DNA binding domain (DBD) common to all nuclear receptors and binds to 9-bp DNA sequences as a monomer. Here we describe the solution structure of the SF1 DBD in complex with an atypical sequence in the proximal promoter region of the inhibin-α gene that encodes a subunit of a reproductive hormone. SF1 forms a specific complex with the DNA through a bipartite motif binding to the major and minor grooves through the core DBD and the N-terminal segment of the FTZ-F1 box, respectively, in a manner previously described for two other monomeric receptors, nerve growth factor-induced-B and estrogen-related receptor 2. However, unlike these receptors, SF1 harbors a helix in the C-terminal segment of the FTZ-F1 box that interacts with both the core DBD and DNA and serves as an important determinant of stability of the complex. We propose that the FTZ-F1 helix along with the core DBD serves as a platform for interactions with coactivators and other DNA-bound factors in the vicinity. (*Molecular Endocrinology* 20: 831–843, 2006)

NUCLEAR HORMONE receptors (NRs) constitute one of the largest families of transcription factors and play important roles in metazoan development and cellular homeostasis by regulating a number of growth and signal transduction pathways (1, 2). The activity of many NRs is regulated by the binding of small lipophilic molecules including steroid hormones, metabolites, lipids, and synthetic ligands. Despite sharing considerable similarities both at the sequence and structural levels, NRs exhibit a high degree of specificity in exerting their physiological effects. Although remarkable progress has been made in the past decade in defining the general principles relating to their mechanism of action at the molecular level, the structural basis for specificity remains poorly understood for many NRs, especially for receptors with no known ligands and/or those that bind DNA as monomers (3).

Steroidogenic factor 1 (SF1/NR5A1) belongs to the NR5A subfamily of NRs that bind DNA as monomers and regulate a number of genes essential for normal reproductive physiology and endocrine function (4, 5). SF1 was originally identified as a homolog of the *Drosophila* NR *fushi tarazu* factor-1 (FTZ-F1/NR5A3) that regulates segmentation (6, 7). SF1 is expressed in the gonads, adrenals, hypothalamus, and pituitary, where it regulates genes encoding steroidogenic enzymes and hormones including FSHβ, LHβ, glycoprotein subunit-α, and Müllerian-inhibiting substance. Mouse SF1 knockouts lead to specific developmental defects including the agenesis of the ovary, testis, and adrenals (8, 9). This is in contrast to its closest homolog and member of the same subfamily, the liver receptor homolog 1 (LRH1/NR5A2), which is expressed in pancreatic, liver, and intestinal tissues and regulates the expression of genes involved in cholesterol metabo-

First Published Online December 8, 2005

Abbreviations: CREB, cAMP response element binding protein; CTE, carboxy-terminal extension; DBD, DNA binding domain; DMT, 5′-dimethoxytrityl; DTT, dithiothreitol; ERR2, estrogen-related receptor 2; GRMO2, ovarian granulosa cells; HRE, hormone response element; LRH, liver receptor homolog; MBF1, multiprotein bridging factor 1; NGFI-B, nerve growth factor-induced-B; NMR, nuclear magnetic resonance; NOE, nuclear Overhauser effect; NR, nuclear hormone receptor; SBS, SF1 binding site; SF1, steroidogenic factor 1.

***Molecular Endocrinology* is published monthly by The Endocrine Society (http://www.endo-society.org), the foremost professional society serving the endocrine community.**

lism (10). LRH1 is also expressed abundantly in the ovary and, like SF1, is proposed to regulate mammalian reproductive function. It also has important roles in early development because LRH1 knockouts are embryonically lethal (11). Recently, both SF1 and LRH1 have been shown to bind phophotidyl inositol ligands, and lipid binding is required for full transcriptional efficacy of these nuclear receptors (12–15).

Members of the NR5A subfamily share the same domain architecture as other NRs although SF1 and FTZ-F1 orthologs lack a transactivation domain N-terminal to the DNA binding domain (DBD). The core DBD shared by all NRs consists of a tandem Cys_4-Cys_4 zinc-finger motif that is essential for the specific recognition of a canonical 6-bp sequence termed the hormone response element [HRE (16–26)]. Unique to the NR5A subfamily is a highly conserved sequence referred to as the "FTZ-F1 box" located immediately C-terminal to the core DBD that is indispensable for high-affinity interactions with DNA [Fig. 1 (27, 28)]. This segment bears limited similarity to an analogous region found in other NRs that bind DNA as monomers including nerve growth factor-induced-B (NGFI-B) and estrogen-related receptor 2 (ERR2). The NR5A members, like these monomeric receptors, have been proposed to recognize a 9-bp sequence comprising a canonical HRE and a 3-bp sequence 5′- to this element. An *in vitro* selection experiment conducted using FTZ-F1 led to the identification of high-affinity binding sites that conformed to the consensus sequence 5′-YCAAGGYCR-3′ [where Y = T/C; R = G/A (29)]. In contrast, several of the natural binding sites on the proximal promoter regions of target genes for SF1 exhibit significant differences from the consensus

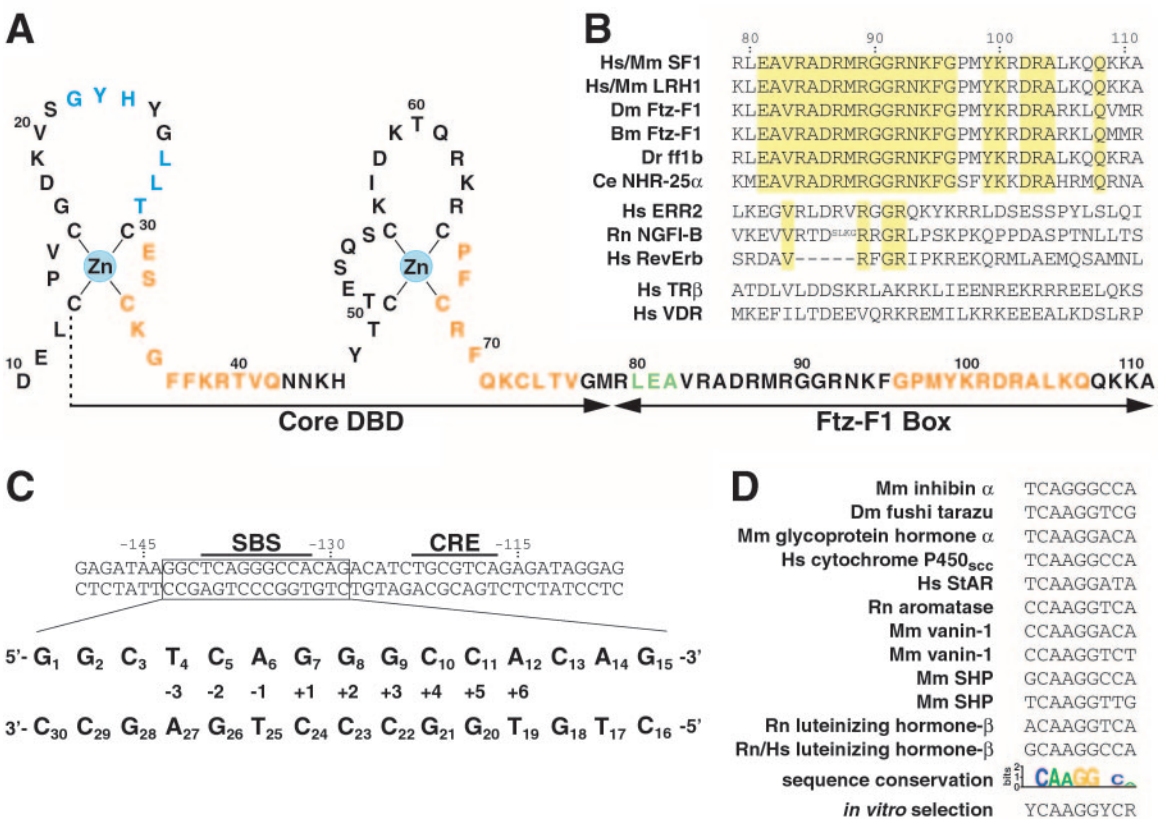

Fig. 1. Analysis of the Protein and Nucleotide Sequences Used in this Study

A, Amino acid sequence corresponding to the Cys_4-Cys_4 zinc finger DBD of mouse SF1. The locations of the highly conserved core DBD shared by NRs as well as the FTZ-F1 box unique to the NR5A subfamily are indicated. SF1 residues found in regular secondary structural elements including α-helices, 3_{10}-helices, and β-strands in the solution structure are colored in *orange*, *green*, and *light blue*, respectively. B, Multiple sequence alignment of the 33-residue FTZ-F1 box found in SF1 homologs. Equivalent C-terminal extensions or CTEs of other structurally characterized receptors are included for comparison. Identical residues are *highlighted*. Species abbreviations: Hs, *Homo sapiens*; Mm, *Mus musculus*; Dm, *Drosophila melanogaster*; Bm, *Bombyx mori*; Dr, *Danio rerio*; Ce, *Caenorhabditis elegans*; Rn, *Rattus norvegicus*. C, The upstream promoter region of the mouse inhibin-α subunit gene encompassing the SBS and the cAMP response element (CRE). Numbering is relative to the transcriptional start site. The 15-bp sequence used for the NMR studies is shown in the *bottom panel*. D, SF1 recognizes a broad range of nucleic acid sequences *in vivo*. A multiple sequence alignment of experimentally characterized SF1 binding sites in the regulatory regions of diverse genes. The proteins encoded by the genes along with the species (same abbreviations as above) in which they are found are identified. Sequence conservation is captured in the form of a logo and is contrasted with the consensus high-affinity binding sequence from an *in vitro* selection procedure. Y, Pyrimidine; R, purine.

(Fig. 1). Another noteworthy feature of SF1 regulation is that many genes appear to be regulated in collaboration with proximally bound, structurally diverse transcription factors including cAMP response element binding protein (CREB), CCAAT-enhancer binding protein (C/EBP-β), pituitary homeobox (Pitx), GATA-4, early growth response protein 1 (EGR-1), β-catenin, estrogen receptor, SRY-box 9 (Sox9), Sp1, and the E2A family of transcription factors (4).

We had previously shown that SF1 plays a role in ovarian follicular function by regulating inhibin (30), a heterodimeric glycoprotein hormone that suppresses FSH secretion in the pituitary (31). We also showed that SF1 activates inhibin-α subunit gene transcription in a synergistic manner with the cAMP-responsive transcription factor CREB, a downstream effector of FSH action (30). Both SF1 and CREB bind to neighboring atypical elements in the proximal promoter region of the inhibin-α subunit gene. To understand the molecular and structural basis for this synergy and to clarify the mode of DNA binding by SF1 and in particular, the role of the FTZ-F1 box, we determined the three-dimensional structure of the SF1 DBD in complex with a 15-bp sequence derived from the inhibin-α-subunit proximal promoter that we refer to as the SBS (SF1 binding site) duplex.

RESULTS

Multiple constructs of mouse SF1 encompassing the core DBD and the FTZ-F1 box were generated, but because of solubility issues, only the shortest construct spanning residues 10–111 was deemed suitable for structural studies. However, at millimolar concentrations required for solution nuclear magnetic resonance (NMR) studies, the protein appeared to form soluble aggregates as indicated by the broad resonance linewidths and poor chemical shift dispersion in the amide region of the ^{1}H NMR spectrum. In contrast, high-quality NMR spectra characterized by excellent chemical shift dispersion and adequate sensitivity was obtained for the SF1 DBD-SBS DNA complex, notwithstanding the atypical nature of the sequence (Fig. 1, C and D). The complex was in slow exchange on the NMR timescale and overall, the spectral characteristics were comparable to those obtained for another SF1 DBD-DNA complex in which the DNA sequence harbored a consensus binding site (see Fig. S1, which is published as supplemental data on The Endocrine Society's Journals Online web site at http://mend.endojournals.org).

Sequence-specific resonance assignments were accomplished using well-established methods and are essentially complete for the DBD. Severe spectral overlap and resonance line broadening for select nucleotides precluded complete assignment of DNA proton resonances. ^{1}H-^{1}H NOESY spectra were of sufficient quality to pursue structure determination using a largely automated approach. An ensemble of 16 structures consonant with the input restraints including no violations above 0.5 Å for distance restraints and above 5 degrees for torsion angle restraints was deemed suitable for further analysis (Table 1).

Overall Structure of the SF1 DBD-SBS DNA Complex

The backbone conformation of the SF1 DBD is defined with reasonable precision by the input restraints but is generally better defined within the core DBD than in the FTZ-F1 box segment. The core DBD of SF1 adopts the well-characterized, zinc-stabilized fold found in other NRs comprising a short β-hairpin near the N terminus, and two α-helices arranged approximately perpendicular to each other separated by a long loop (Fig. 2). The N-terminal half of the FTZ-F1 box immediately after the core DBD adopts a conformation comprising a 3_{10}-helix and a succession of turns akin to those found in the CTEs (carboxy-terminal extensions) of the monomeric receptors NGFI-B and ERR2 (20, 25). A distinctive feature of the FTZ-F1 box is the presence of an additional α-helix in the C-terminal half of the segment that we designate the FTZ-F1 helix. The SBS DNA duplex conformation is essentially B-form, and the backbone precision is better for those regions in close proximity to the protein than otherwise.

The first helix in the core DBD of SF1 docks into the major groove of the DNA and serves as the primary recognition module for the atypical HRE in the SBS. The FTZ-F1 box provides a secondary recognition element by crossing over to the minor groove and engaging the sequence immediately 5′ to the HRE. One end of this element is anchored by the FTZ-F1 helix through long-range noncovalent interactions.

Intermolecular Interactions between SF1 DBD and the SBS Duplex

Noncovalent interactions stabilizing the SF1 DBD-SBS DNA complex largely mimic the general trend observed for other NR-DNA complexes. Figure 3 catalogs the intermolecular hydrogen bonding and electrostatic interactions that are consistently detected in the majority of the structures comprising the NMR ensemble. A Glu-Lys pair consisting of Glu31 and Lys34 near the N terminus of the recognition helix (a region widely referred to as the "P-box") makes base-specific hydrogen bonding interactions with two consecutive G:C base pairs at the +2 and +3 positions in the HRE (Fig. 3). These interactions are bolstered by additional hydrogen bonds between Lys38 Nζ and Gua9 N7 (at the +3 position in the HRE) and also between Arg39 Nη and Gua20 O6 (+5 position). Because the terminal groups in the Lys38 and Arg39 side chains are somewhat disordered, these interactions are not consistently detected in the NMR structures. An impressive array of nonspecific interactions involv-

Table 1. NMR Structure Determination Statistics

Structure	Value
Restraint statistics	
Distance restraints	
Unambiguous NOE-based restraints	2263
Intraresidue	1111
Sequential ($\mid i - j \mid = 1$)	530
Medium-range ($1 < \mid i - j \mid \leq 4$)	228
Intramolecular long-range ($\mid i - j \mid > 4$)	335
Intermolecular	59
Ambiguous NOE-based restraints	532
Intramolecular NOE-based restraints	297 DNA, 2439 protein
Hydrogen bonding restraints	118
Metal coordination restraints	20
Torsion angle restraints	
Protein backbone ϕ and ψ restraints	116
DNA backbone and glycosidic restraints	200
Tetrahedral metal coordination restraints	2
Structure quality of NMR ensemble	
Restraint satisfaction	
RMS differences for distance restraints	0.015 ± 0.001 Å
RMS differences for torsion angle restraints	0.235° ± 0.050°
Deviations from ideal covalent geometry	
Bond lengths	0.003 ± 0.000 Å
Bond angles	0.439° ± 0.012°
Impropers	0.963° ± 0.047°
Ramachandran plot statistics[a]	
Residues in most favored regions	80.8%
Residues in additionally allowed and generously allowed regions	17.2%
Residues in disallowed regions	2.0%
Average atomic RMSDs from the average structure	
All atoms[a]	2.01 Å
All atoms except residues at chain termini[b]	1.62 Å
Backbone atoms (N, C^{α}, C′, P, O5′, C5′, C4′, C3′, O3′)	
All residues[a]	1.64 Å
All residues except residues at chain termini[b]	1.17 Å
Residues in the core DBD[c] and 9-bp SBS	0.98 Å
Residues in the core DBD[c]	0.67 Å

RMS, Root mean square; RMSD, RMS deviation.

[a] Excluding 23 residues in the nonnative sequence N-terminal to the SF1 DBD.

[b] Excludes the three terminal base pairs flanking the SBS and residues 10–12, 107–111 of SF1.

[c] Core DBD comprises residues 13–78 of SF1.

ing main chain amides (Tyr25 and Arg84) as well as side chain hydroxyl, imidazole, amino, and guanidium groups with backbone phosphate groups in the DNA are detected (Fig. 3). These interactions are especially concentrated in a region where residues from the β-hairpin, the C terminus of the recognition helix, and the FTZ-F1 box congregate near one strand of the DNA. Similar backbone interactions involving two spatially proximal arginines (Arg62 and Arg69) with the other DNA strand are also detected.

There are surprisingly few well-defined, base-specific interactions involving the RGGR motif in the FTZ-F1 box in the SF1 DBD-DNA complex (Fig. 3). Identical or similar motifs have been implicated in such interactions in other monomeric NR-DNA structures. This is attributed to the modest to severe resonance broadening effects associated with residues within the motif as only a handful of intermolecular nuclear Overhauser effects (NOEs) involving the arginine residues were detected. Interestingly, in the atypical SBS sequence found in the inhibin-α promoter, a G:C base pair replaces an A:T base pair that would normally make contacts with one of the arginine side chains (Arg89).

Packing and Noncovalent Interactions of the FTZ-F1 Helix

A unique feature of the SF1 DBD-DNA complex is the presence of an additional helix after the RGGR motif. The FTZ-F1 helix, which encompasses residues Phe95 to Gln107, extends from one edge of the minor groove to the other and beyond while simultaneously engaging the core DBD. The helical axis is almost in the same plane as the A6:T25 base pair and approximately parallel to the C1′-C1′ vector of this base pair (Fig. 2B).

The side chain conformations in the helix are generally less well defined than those in the core of the DBD. However, residues at the N terminus of the helix including Phe95, Met98, and Tyr99 define a mini hy-

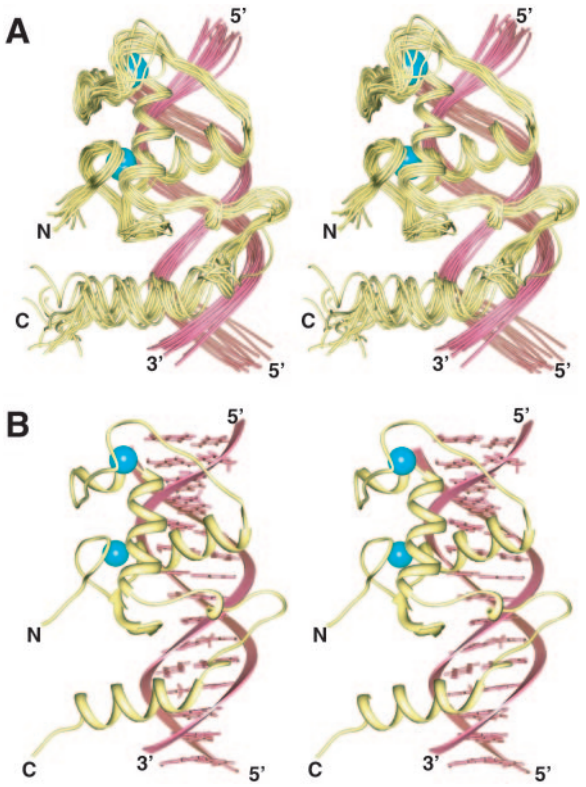

Fig. 2. Cross-Eyed Stereographic Views of the Solution Structure of the SF1 DBD-SBS DNA Complex

A, A best-fit superposition of the backbone atoms in the ensemble of 16 structures highlighting the precision with which the various segments of the complex are determined by the NMR data. The polypeptide (*beige*) and nucleic acid (*magenta*) backbones are drawn as smoothed splines, whereas the zinc atoms are shown as spheres (*cyan*). B, A representative structure from the ensemble illustrating the location of the various secondary structural elements. Bases in the SBS duplex are shown in a stick representation. N, Amino terminus; C, carboxy terminus.

drophobic core that packs against the backbone in the turn region between the β-strands and also the N-terminal segment of the FTZ-F1 box (Fig. 4). The hydroxyl group of Tyr99 is within hydrogen bonding distance of backbone donor and acceptor groups in the β-hairpin region of the core DBD. In some structures, it is also in a position to form hydrogen bonds with the A6 O3′ and G7 phosphate oxygen atoms. Another hydrogen bonding interaction that is consistently detected in the NMR structures involves the hydroxyl group of Tyr23 and the carboxyl moiety of the Asp102. Poorly defined are electrostatic interactions involving the side chains of Lys100 and Arg103 with the backbone phosphate groups of the DNA and those between the side chains of Lys106 and Glu13 in the core DBD.

Functional Implications of SF1 DBD Mutations

To assess the contributions of various SF1 DBD residues toward DNA binding and transactivation, a panel of mutants in the context of the full-length SF1 protein was generated and tested in transient transfection assays. Residues in the core DBD, the RGGR motif, and the FTZ-F1 helix were mutated including those that 1) engaged in specific interactions with DNA, 2) interacted with the sugar-phosphate backbone in a nonspecific manner, 3) were at the protein-DNA interface but whose interactions with DNA were ambiguous, and 4) were far removed from the protein-DNA interface. The assays employed a luciferase reporter downstream of a promoter element from the inhibin-α-subunit gene harboring the atypical SBS and were conducted in immortalized ovarian granulosa cells (GRMO2). None of the mutants tested impaired the ability of the inhibin α reporter to respond to forskolin stimulation, indicating that CREB-mediated transcription of the gene is not impaired by the mutant SF1 proteins (data not shown).

Alanine mutations of class 1 residues including Glu31, Lys34, Lys38, and Arg39 significantly diminished the transactivation potential of the mutant proteins (Fig. 5A, *top panel*). In contrast, the class 2 Lys63Ala and Arg87Ala mutants exhibited robust levels of activation, whereas the class 4 mutants including Leu80Lys and Met98Ala also shared this trait. The only class 4 mutant that exhibited greatly diminished transcriptional activity compared with wild-type SF1 was the Arg101Pro, Asp102Pro double mutant, which was designed to perturb the FTZ-F1 helix. Interestingly, alanine mutations of two class 3 residues Arg89 and Arg92, both of which belong to the RGGR motif, yielded contrasting results. Although the Arg89Ala mutant exhibited robust transactivation, the Arg92Ala mutant failed to activate significantly above basal levels. The two other class 3 mutants Tyr99Ala and Tyr99Phe, designed to perturb the interactions involving the aromatic side chain also failed to activate transcription significantly over basal levels. It is unlikely that the inability or diminished ability of some of these mutants to transactivate is explained by rapid protein turnover as Western blot analysis indicated that all the alanine substitution mutants, with the exception of the Arg39Ala and Tyr99Ala mutants, appeared to express well and at equivalent levels in transfected HeLa cells (Fig. 5A, *bottom panel*).

To evaluate the contribution of the FTZ-F1 helix toward the stability of the SF1 DBD-DNA complex, the transactivation potential of two FLAG-tagged SF1 constructs harboring an internal deletion spanning residues Pro97 to Ala111 in the FTZ-F1 box (designated SF1 Δ97–111) was tested in transient transfection assays. Interestingly, these mutants showed only basal levels of activation, whereas the FLAG-tagged wild-type full-length SF1 proteins showed comparable activity as the untagged wild-type full-length SF1 (Fig. 5B, *top panel*). Because the mutant proteins were readily detected in Western blots, it is unlikely that the loss of activity is caused by rapid protein turnover (Fig. 5B, *bottom panel*).

Because several mutants targeting residues in the FTZ-F1 helix, including Tyr99Ala, Tyr99Phe, Arg101Pro,

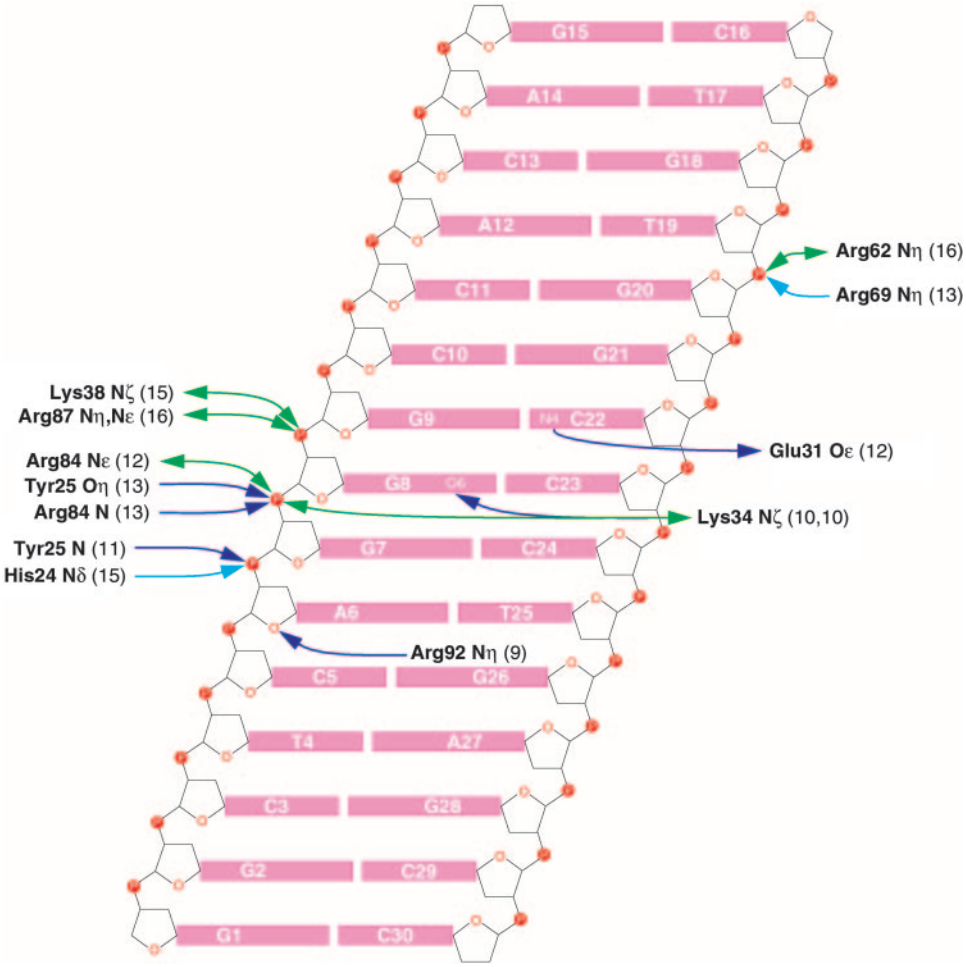

Fig. 3. A Catalog of All Intermolecular Hydrogen Bonding (*Blue*) and Electrostatic (*Green*) Interactions in the SF1 DBD-SBS DNA Complex that Are Observed in the Majority of Structures in the NMR Ensemble

The heavy atoms involved in these pairwise interactions are shown, whereas *the numbers in parentheses* indicate the number of structures in the ensemble in which the interaction is detected. For hydrogen bonding interactions, donors and acceptors are distinguished by the direction of the *arrow*. Salt bridges are shown in *cyan*.

Asp102Pro, and Δ97–111 exhibited considerably diminished activity in transcription assays, we sought to test their ability to bind DNA *in vitro*. EMSAs were used to monitor DNA binding as a function of concentration over a 30-fold range of added protein. A quantitative analysis of the binding affinities, especially for the wild-type SF1 DBD, was not possible because the binding isotherms exhibited significant deviations from normal hyperbolic profiles expected for monomer binding. This is attributed to the protein's tendency to aggregate readily over a broad range of solution conditions and precipitate in the presence of modest amounts of salt (~0.1 M) and at basic pH. We have therefore sought to compare DNA binding activities in qualitative terms. The mobility shift assays were conducted using bacterially expressed and purified wild-type SF1 DBD and the four FTZ-F1 helix mutants employing oligonucleotide probes harboring either atypical or consensus SF1 binding sites. The atypical site contains the inhibin-α-subunit sequence used for the structural studies. All four mutants bound to the consensus sequence with lower affinity compared with the wild-type protein and in the order Arg101Pro, Asp102Pro > Tyr99Phe ~ Tyr99Ala ≫ Δ97–111 (Fig. 6A). Significantly, binding to the atypical sequence was attenuated for all the proteins tested including the wild-type SF1 DBD, but even more so for all the mutants (Fig. 6B). These observations are in complete agreement with the results from transcriptional assays that were also conducted with the atypical sequence (Fig. 5).

DISCUSSION

Despite sharing extensive sequence similarity, NRs exhibit significant diversity in their modes of sequence-specific DNA recognition. High-resolution structures of about a dozen different NR DBD-DNA complexes confirm the essential nucleating role of the core DBD in recognizing the canonical HRE (16–26).

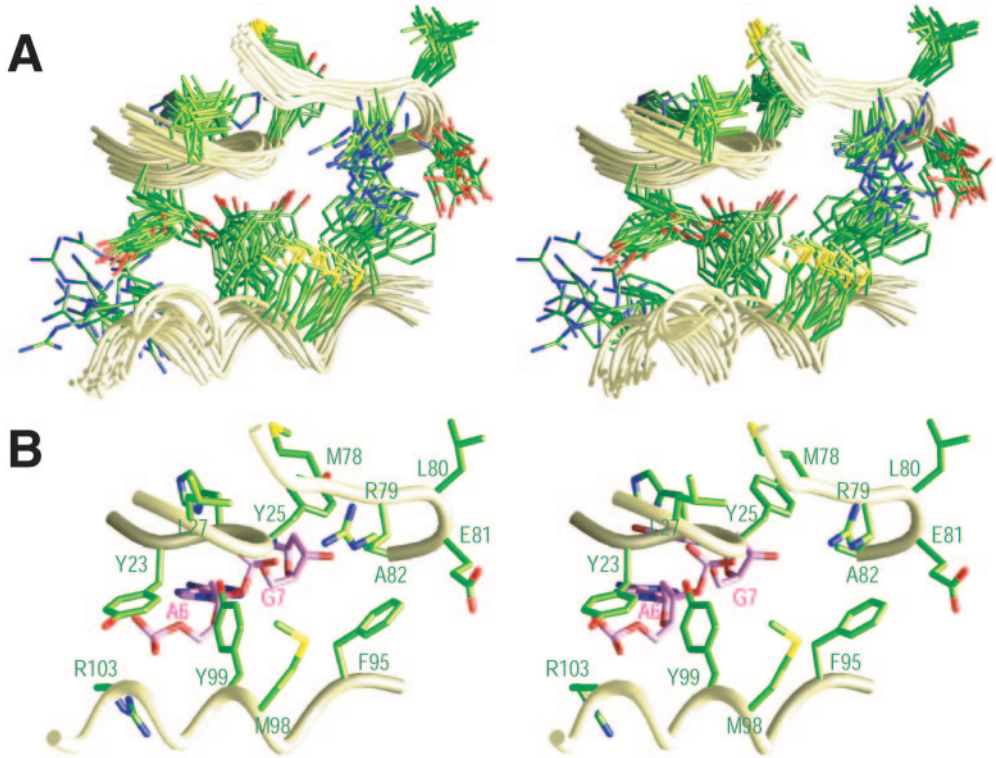

Fig. 4. Packing Interactions Involving the C-Terminal Helix of SF1 DBD with the Core DBD and the N-Terminal Region of the FTZ-F1 Box

A, An ensemble-wide, all-atom best-fit superposition of selected residues in the SF1 DBD emphasizing the precision with which the side chain conformations are defined by the NMR data. B, The corresponding backbone and side chains of a representative structure from the ensemble are shown along with nucleotides in close proximity to Tyr99.

However, this alone is insufficient for high-affinity interactions. Oligomerization and cooperativity involving segments within the core DBD and/or the CTE are key for ensuring high-affinity NR-DNA interactions. The CTE also plays an important role in monomeric NR-DNA interactions by extending the protein-DNA interface to the minor groove. However, similarities and important variations are beginning to emerge between various monomeric NR DBD-DNA complexes.

Comparison with Other NR DBD-DNA Interactions

The DBD of SF1 shares grossly similar features both at the backbone and the side chain levels with the NGFI-B and ERR2 DBDs (20, 25). Indeed, a representative structure of SF1 DBD superimposes with the NGFI-B and ERR2 DBDs leading up to a few residues past the 3_{10}-helix with backbone root mean square deviations in the 1.2-Å range. Differences in the trajectories of the respective backbones beyond this point become more readily apparent but are particularly pronounced past the RGGR/RGR motifs. Interestingly, residues in the segment C-terminal to the RGGR motif in both SF1 and ERR2 engage the core DBD, whereas a comparable interaction is completely absent in NGFI-B, which harbors an alternative RGR motif. Another noteworthy parallel between SF1 and ERR2 is the structural role played by a tyrosine residue (Tyr99 and Tyr185, respectively) in anchoring the C-terminal segment to the core DBD. Tyr99 is seven residues removed from the RGGR motif, whereas the functionally equivalent Tyr185 is only three residues C-terminal to the RGGR motif in the respective proteins. However, unlike the side chain of Tyr185 in the ERR2 DBD-DNA complex, the side chain of Tyr99 in the SF1 DBD-DNA complex is closer to and most likely interacts with the sugar-phosphate backbone of the DNA (Fig. 4).

Recognition of an Atypical Physiologically Relevant Sequence

An interesting aspect of the DNA sequence employed in this study is that it is a lower-affinity target for SF1. Many physiologically important target genes harbor such atypical SF1 binding sites (Fig. 1D). The low-affinity SF1 binding of the inhibin-α- subunit SBS sequence is confirmed by the results of our comparative DNA binding assays conducted with this same sequence and a sequence conforming to the consensus SF1 binding sequence (Fig. 6). The replacement of an A:T base pair at the $+1$ position by a G:C base pair appears to have an effect on the structure and internal dynamics of the complex. For example, the guanine

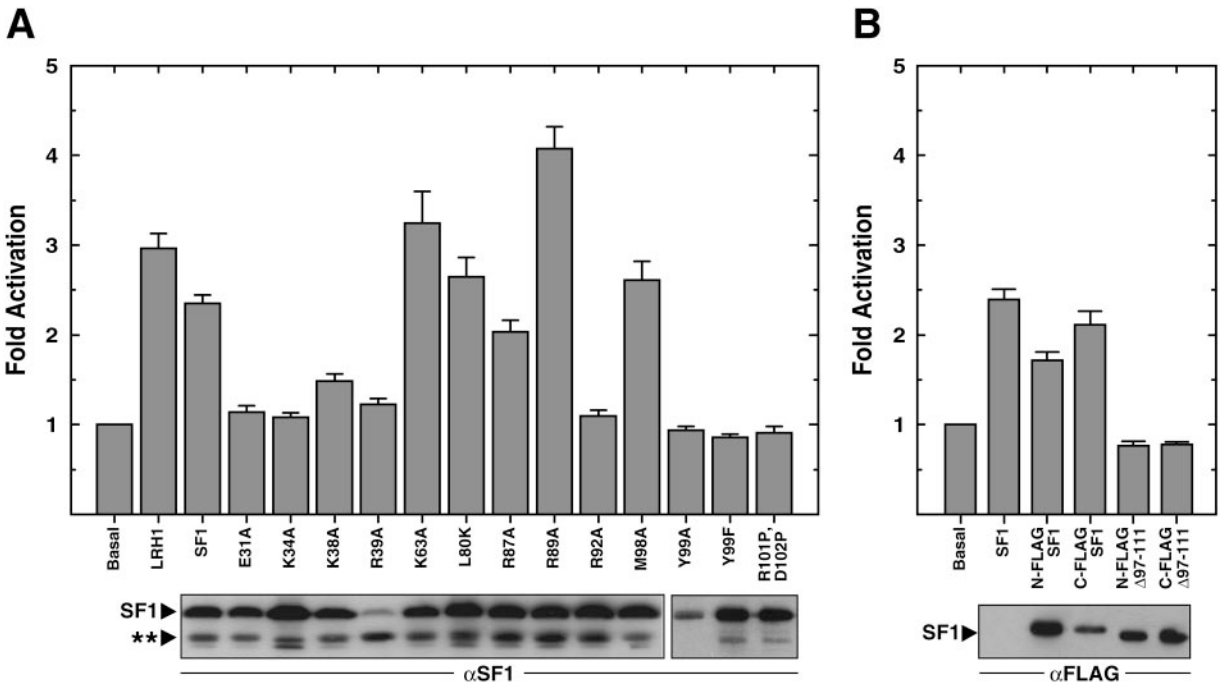

Fig. 5. Effects of Mutations in the DBD on the Transactivation Potential of SF1

A, Transient transfection assays conducted in GRMO2 cells using wild-type and mutant full-length SF1 and LRH1 proteins and a luciferase reporter gene located downstream of a promoter element (−547 to +63) from the inhibin-α subunit gene (*top panel*). The fold-activation was computed relative to basal reporter activity. *Error bars* represent the standard error of measurements (n = 6–22). Western blot analysis of the wild-type and mutant proteins expressed in HeLa cells and probed with an anti-SF1 antibody after SDS-PAGE separation. The bands denoted by *asterisks* likely correspond to degradation products. B, Transient transfection assays conducted in GRMO2 cells using wild-type full-length SF1 and FLAG-tagged wild-type and mutant SF1 constructs and using the same reporter as in A. *Error bars* represent the SE of measurements (n = 4). Western blot analysis of the corresponding proteins expressed in HeLa cells and probed with an anti-FLAG antibody after SDS-PAGE separation.

amino group, through steric clashes, likely precludes the side chain of Arg89 from making base-specific contacts. The equivalent arginine residue, Arg179 in ERR2 was implicated in hydrogen bonding interactions with the thymine O_2 moiety of the A:T base pair at the +1 position (25). The suboptimal context of the G:C base pair in the SF1 DBD-DNA complex likely contributes to some of the severe resonance broadening effects associated with the residues in this region including the RGGR motif in the DBD. Future NMR studies of a consensus SBS-SF1 DBD complex should help clarify this further.

Notwithstanding the suboptimal nature of the DNA sequence, the SF1 DBD appears to form a specific complex as residues implicated in making base-specific contacts by the structural analysis strongly diminish the transactivation potential of SF1 in transfection assays (Fig. 5). Interestingly, the latter studies also suggest a nonessential role for Arg89 in the RGGR motif, at least vis-à-vis the recognition of the atypical SBS. By contrast, Arg92 appears to play an important role in this regard.

Role of the FTZ-F1 Helix in Complex Stability and Transcription Factor Interactions

Perhaps the most distinctive feature of the SF1 DBD is the presence of an α-helix at the C terminus of the domain. Although an α-helix in the CTE has also been reported for the thyroid hormone and vitamin D receptors (18, 23), the packing and relative orientation of the helix with respect to the core DBD and DNA are completely different. In the SF1 DBD-DNA complex, residues in the FTZ-F1 helix not only engage in long-range noncovalent interactions with the core DBD, a few of them also are in a position to make nonspecific contacts with the DNA. All of these interacting residues are either invariant or highly conserved in the NR5A subfamily (Fig. 1B). The results from transient transfection as well as DNA binding assays confirm the important role of the helix toward complex stability as perturbation of the helix through proline substitutions or deletion of the entire helix adversely affects the normal function of SF1 (Figs. 5 and 6). The transcription and DNA binding assays also highlight the crucial role of the tyrosine residue (Tyr99) in the helix, and particularly its hydroxyl moiety, as mutation to phenylalanine or alanine negatively affects SF1 function. Finally, it is plausible that the FTZ-F1 helix is a particularly important determinant in allowing SF1 to effectively bind to and activate a broad range of target genes that exhibit substantial variability in the SF1 recognition sequence (compare Fig. 6, A and B).

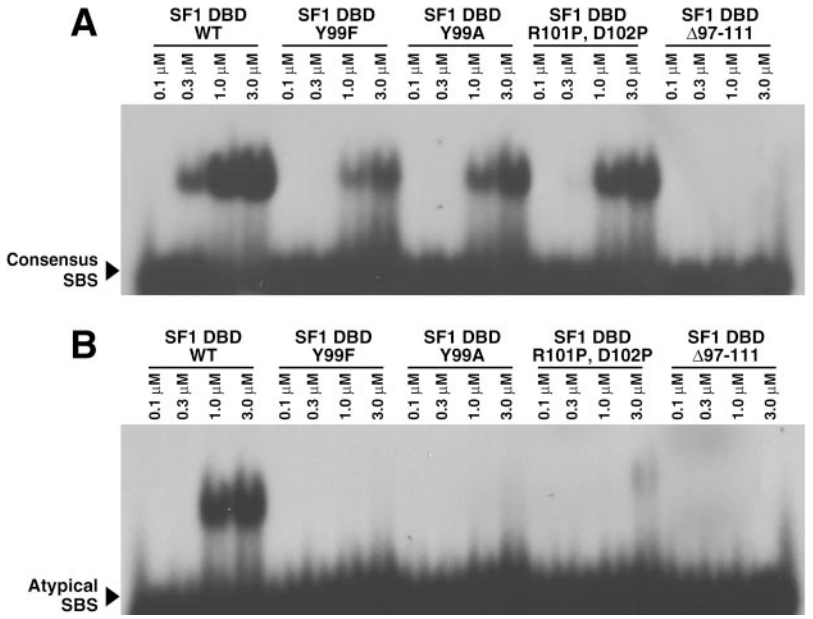

Fig. 6. Analysis of the Stabilities of a Panel of SF1 DBD-DNA Complexes

A, EMSAs conducted as a function of increasing concentrations of wild-type and mutant SF1 DBD with an oligonucleotide probe harboring a consensus SF1 binding site. The proteins used in these assays were expressed in bacteria, purified, and rigorously quantified before being employed in the binding assays. B, Analogous EMSAs conducted using the same proteins, but with an atypical SBS.

Interestingly, SF1 and FTZ-F1 DBD mutants lacking the FTZ-F1 helix region have been reported to bind consensus DNA sequences with similar affinities as the wild-type proteins (27, 28). The apparent discrepancy with our findings is not clear, but one likely explanation is that the assays were performed at concentrations much higher than the dissociation constants of the respective complexes, effectively precluding clear discrimination between their binding affinities.

The FTZ-F1 box has been proposed to play a role in NR5A-mediated transactivation by serving as a site for tethering other transcription factors. A particularly well-studied example is a transcriptional coactivator called the multiprotein bridging factor 1 (MBF1) that interacts with multiple factors including the TATA binding protein (32–35). The interaction between NR5A proteins and MBF1 as well as MBF1-dependent coactivation relies on an intact FTZ-F1 helix and also on the presence of basic residues within the helix (33). These results when considered in light of the important role performed by the helix in stabilizing the structure of the DBD-DNA complex suggest that a potential MBF1 interacting surface could involve: 1) the FTZ-F1 helix itself as a direct and exclusive target, 2) a site completely distinct from the FTZ-F1 helix that nonetheless relies on the helix for proper folding of the DBD, or 3) a site that partially overlaps with the FTZ-F1 helix. We note that the surface adjacent to the FTZ-F1 helix of SF1 DBD is dominated by hydrophobic residues (Fig. 7) and could be a site for interactions with MBF1 and possibly other transcription factors. Because MBF1 has also been proposed to interact with the basic region of basic-leucine zipper transcription factors, one model for the observed synergy between SF1 and CREB in activating inhibin-α-subunit gene transcription could result from the stabilization of a multiprotein-DNA complex with MBF1 serving as a molecular adapter linking these factors through protein-protein interactions.

Crystal Structure of Human LRH1 in Complex with DNA

After the initial submission of this manuscript, the crystal structure of human LRH1 in complex with DNA has been reported (36). The principal conclusions from that study on a related NR5A protein are in accord with those described in this paper. It appears that ERR2, SF1, and LRH1 comprise a growing list of monomeric receptors, with the exception of NGFI-B, that rely on long range packing interactions between residues in the CTE and the core DBD.

Materials and Methods

Expression and Purification of SF1 DBD

The coding sequence of the mouse SF1 DBD corresponding to amino acids 10–111 was amplified by PCR and inserted into the pMCSG7 expression vector (37). *E. coli* BL21(DE3) cells (Novagen, Madison, WI) containing the vector were grown at 37 C in M9 minimal media supplemented with 50 μM $ZnCl_2$. The growth temperature was shifted to 20 C when the $OD_{600\ nm}$ reached approximately 0.7. Protein expression was induced using 1 mM isopropyl-β-D-thiogalactopyranoside, and the cells were harvested 16 h thereafter. Cell pellets were suspended in

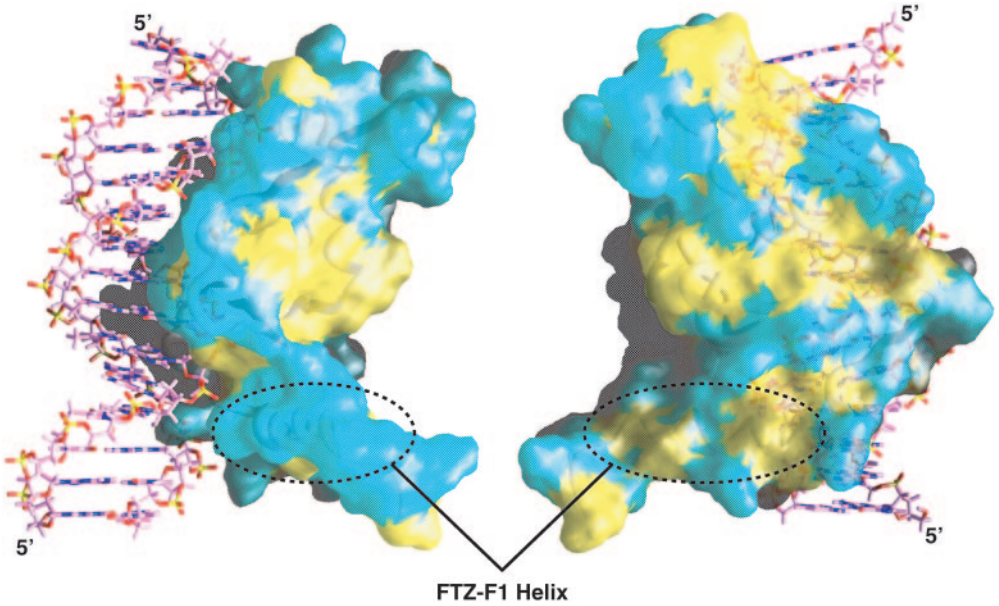

Fig. 7. A Hydrophobic Patch in the Vicinity of the FTZ-F1 Box Helix of SF1 DBD as a Potential Platform for the Assembly of Additional Factors

Two views of the protein-DNA complex with the DBD rendered as a molecular surface and the DNA drawn in a stick representation. Hydrophobic regions (Ala, Cys, Phe, Ile, Leu, Met, Pro, Thr, Val, Trp, and Tyr) of the surface are colored *yellow*, whereas the hydrophilic regions (Asp, Glu, Gly, His, Lys, Asn, Gln, Arg, and Ser) are colored *cyan*. The surface is rendered semitransparently so that the polypeptide backbone can be seen. The location of the FTZ-F1 helix is indicated.

20 mM sodium phosphate buffer (pH 7.2) containing 500 mM NaCl, 50 μM $ZnCl_2$, 2 mM Tris(2-carboxyethyl) phosphine, 1 mM phenylmethylsulfonyl fluoride, 1 μM leupeptin, 1 mM pepstatin, and 0.1% Triton X-100. The cells were lysed via sonication and the protein was purified from both the soluble and insoluble (solubilized in 8 M urea) fractions using His-Select Nickel Affinity Gel (Sigma, St. Louis, MO). Bound proteins were eluted with buffer containing 500 mM imidazole. SF1 DBD-containing fractions were further purified using reversed-phase HPLC using a C18 column (Vydac, Hesperia, CA) and a mobile phase comprising 80% acetonitrile and 0.1% trifluoroacetic acid and lyophilized. SF1-DBD samples uniformly labeled with ^{15}N and/or ^{13}C isotopes were produced as described above, except that cells were grown in M9 minimal media containing ^{15}N-ammonium sulfate and/or ^{13}C-D-glucose (Spectra Stable Isotopes, Columbia, MD), respectively. The identity of the protein as well as the extent of isotope enrichment (typically, ^{15}N >98% and ^{13}C >97%) was confirmed by electrospray ionization mass spectrometry.

Production and Purification of DNA Oligomers

Complementary single-stranded oligodeoxyribonucleotides harboring the SBS in the inhibin-α promoter were purchased from Trilink Biotechnologies Inc. (San Diego, CA) with an intact 5′-dimethoxytrityl (DMT) group. Sequences with the DMT group were isolated via reversed-phase HPLC (Vydac C4 column) using a mobile phase comprising 80% acetonitrile and 0.1 M triethylammonium acetate buffer (pH 6.5). The DMT group was removed using 80% acetic acid and the oligomers purified by another round of reversed-phase HPLC. Purified single-stranded oligomers were combined, lyophilized, redissolved in water, and desalted using a Sephadex G25 column (GE Healthcare, Piscataway, NJ). The complementary strands were combined in an equimolar ratio, based on concentrations determined from $A_{260\ nm}$ measurements, heated to 65 C and annealed. The 1:1 stoichiometry of the two strands was verified by recording ^1H NMR spectra.

SF1 DBD-SBS Complex Generation and NMR Sample Preparation

Lyophilized SF1 DBD and SBS duplex were dissolved separately in 10 mM Tris-d_{11} acetate-d_4 NMR buffer (pH 6.0) containing 50 μM $ZnCl_2$ and 2 mM dithiothreitol-d_{10}. Equimolar complexes of ^{15}N- or ^{15}N,^{13}C-labeled SF1 DBD and SBS were generated by titrating the interacting components at 40 μM concentration. The progress of the titration was followed by monitoring the disappearance of free SBS resonances in the imino proton region of the ^1H NMR spectrum. The samples were concentrated by ultrafiltration using a Centriprep-3 to approximately 0.5–1 mM for NMR experiments. During this process, 0.2% (wt/vol) NaN_3 and 1% (vol/vol) glycerol-d_8 were added for conferring additional stability to the sample.

NMR Spectroscopy and Structure Determination

All NMR data were acquired at 35 C on a Varian Inova 600 MHz spectrometer. NMR data processing and analyses were performed using an in-house modified version of Felix98 [Accelrys (38)]. Backbone and side chain ^1H, ^{15}N, and ^{13}C resonances for SF1 DBD were assigned from three-dimensional (3D) HNCA, HN(CO)CA, HNCACB, CBCA(CO)NH, C(CO)NH-TOCSY, H(CCO)NH-TOCSY, HNCO, HCACO, ^{15}N-edited TOCSY, HCCH-COSY, and HCCH-TOCSY spectra (39, 40). Aromatic resonances were assigned from 2D (HB)CB(CGCDCE)HD and (HB)CB(CGCDCE)HE spectra (41). SBS DNA proton resonances were assigned from 2D ^{15}N,^{13}C-double-half-filtered NOESY and TOCSY spectra (42).

NMR Structure Determination

Structures were calculated using ARIA version 1.2 in combination with CNS (43, 44). NOE restraints were obtained from 3D ^{15}N-edited NOESY (mixing time, τ_m= 80 ms), 3D aliphatic and aromatic ^{13}C-edited NOESY (τ_m= 60 and 80 ms, respectively), 3D ^{13}C-filtered, ^{13}C-edited NOESY [τ_m= 120 msec

(45)], and 2D ^{15}N,^{13}C-double-half-filtered NOESY (τ_m= 120 msec) spectra recorded in H_2O and D_2O. Intermolecular NOEs were assigned manually and were calibrated indirectly by calculating a scaling factor for the intensities of well-resolved peaks in ^{13}C-edited NOESY and ^{13}C-filtered, ^{13}C-edited NOESY spectra. These NOEs were assigned upper bounds of 3.6, 4.5, 5.4, and 6 Å. All other NOEs were calibrated automatically and assigned iteratively by ARIA. All NOEs as well as resonance assignments were checked manually for errors after every refinement cycle.

Polypeptide backbone ϕ and ψ torsion angle restraints were derived from an analysis of H^{α}, C^{α}, C^{β}, C', and backbone ^{15}N chemical shifts using TALOS (46). Nucleic acid backbone α, β, γ, ϵ, and ζ torsion angles were restrained to broad ranges found in canonical A- and B-form DNA (47). The χ and δ torsion angles were also loosely restrained to the *anti* and *C2′-endo* ranges, respectively. Hydrogen bonding distance restraints between donor-acceptor pairs were included to maintain Watson-Crick base pairing. Analogous distance restraints were introduced within segments of the DBD deemed to be helical from chemical shift and NOE analyses. Metal-sulfur and sulfur-sulfur distance and torsion angle restraints were included for maintaining the tetrahedral coordination geometry of Zn^{2+} ions.

Structures were calculated from extended backbone conformations as starting models. The Cartesian dynamics option was used for a two-stage simulated annealing protocol with initial temperatures set to 4000 and 2000 K and final force constants for the distance and torsion angle restraints set to 50 kcal $mol^{-1}Å^{-2}$ and 200 kcal mol^{-1} rad^{-2}, respectively. NOEs were assigned after the default ARIA nine-iteration scheme. Forty structures with the lowest restraint energies were subjected to another iteration of simulated annealing starting at 500 K. The simulations were conducted with a shell of explicit solvent and with the inclusion of electrostatics and van der Waals terms in the potential energy function. In all but the final iteration, the DNA was harmonically restrained to standard B-form conformation. Sixteen structures with the lowest restraint energies, restraint violations, and backbone root mean square deviations from ideal covalent geometry were selected for further analysis. The quality of the final structures was analyzed using CNS (44) and PROCHECK (48), noncovalent interactions were analyzed using MONSTER (49) and PROMOTIF (50) and molecular images were generated using CHIMERA (51) and GRASP (52).

Generation of Mutants

Mutants of full-length SF1 or SF1 DBD were engineered using the QuikChange site-directed mutagenesis kit (Stratagene, La Jolla, CA). FLAG-tagged, full-length SF1 wild-type and Δ97–111 mutant constructs were generated by inserting the coding sequence for DYKDDDDK either immediately after the start codon or immediately before the stop codon. All mutations were confirmed by DNA sequencing. Mutant SF1 DBD proteins were expressed in bacteria and purified using analogous approaches used for producing wild-type DBD except for the omission of the final reversed-phase HPLC step.

Transient Transfection and Luciferase Assays

GRMO2 cells were cultured as previously described (53, 54) in HDTIS buffer [1:1 mixture of Ham's F-12 medium (Invitrogen Life Technologies, Carlsbad, CA) and DMEM, 5 μg/ml transferrin, 10 μg/ml insulin, and 5 nM sodium selenite] supplemented with 2% fetal bovine serum and sodium pyruvate (100 mg/liter) in a humidified incubator at 37 C and 5% CO_2. The cells were transfected with a −547 inhibin-α-Luc reporter DNA (500 ng) and full-length SF1 wild-type or mutant expression constructs (10 ng) for each well of a 12-well culture dish (55, 56). The DNAs were incubated at room temperature with lipofection reagent for 20 min in OptiMEM. Cells were washed with PBS, incubated with the DNA-lipid mixture for 6 h, then maintained in fresh HDTIS containing 2% fetal bovine serum for 14–16 h. Cells were washed twice with PBS and lysed on ice in lysis buffer [25 mM HEPES (pH 7.8), 15 mM $MgSO_4$, 1 mM dithiothreitol (DTT), and 0.1% Triton X-100]. Cell lysates (100 μl) were added to 400 μl reaction buffer [25 mM HEPES (pH 7.8), 15 mM $MgSO_4$, 5 mM ATP, 1 μg/ml BSA, and 1 mM DTT] containing 100 μl 1 mM luciferin (Analytical Bioluminescence), and the emitted luminescence was measured for 10 sec using an Analytical Bioluminescence (San Diego, CA) Monolight 2010 Luminometer (57). Relative light units were normalized for total protein content. Protein concentrations were estimated via a Bradford colorimetric assay (Bio-Rad, Hercules, CA) using 5–8 μl of cell lysate.

Preparation of Whole-Cell Protein Extracts and Western Blot Analysis

HeLaT4 cells were cultured in DMEM supplemented with 5% fetal bovine serum in a humidified incubator at 37 C and 5% CO_2. The vaccinia T7 RNA polymerase hybrid expression system was used to overexpress the full-length SF1 wild-type and mutant proteins from the vector pCMX (58). Cultured cells were washed with PBS, centrifuged, resuspended in lysis buffer [50 mM Tris (pH 7.4), 1% NP-40, 0.25% sodium deoxycholate, 150 mM NaCl, 1 mM EGTA, 1 mM phenylmethylsulfonyl fluoride, 1 μg/ml each of antipain, aprotinin, leupeptin, and pepstatin, and 1 mM NaF], incubated on ice and lysed by two freeze-thaw cycles. Lysates were centrifuged and the supernatant was frozen at −80 C. Soluble proteins in the lysate were resolved by SDS-PAGE, transferred to nitrocellulose, blocked with 3% BSA, incubated with a primary anti-SF1 antibody (catalog no. 06-431; Upstate Biotechnology, Lake Placid, NY) at 1 μg/ml or anti-FLAG antibody (Sigma F-3165) at 0.17 μg/ml for 2 h at room temperature, washed with TBS, incubated for 1 h at room temperature with donkey antirabbit antibody (for the primary anti-SF1 antibody) conjugated to horseradish peroxidase (1:10,000; Amersham Biosciences, Piscataway, NJ) or with sheep antimouse antibody (for the primary anti-FLAG antibody) conjugated to horseradish peroxidase (1:6000; Amersham Biosciences) in 10% dry milk in TBS with gentle rocking. The blot was washed with TBS containing 0.1% Tween and the antibody-antigen complexes were visualized using an enhanced chemiluminescence system (ECL Plus Kit, Amersham Biosciences).

EMSAs

Complementary oligonucleotides corresponding to −141 to −118 of the inhibin-α-subunit gene (designated atypical SBS = 5′-TAAGGC**TCAGGGCCA**CAGACATCTGCGTCAGAGATA) or to the same region but containing a consensus SF1 binding site (consensus SBS = 5′-TAAGGC**TCAAGGTCA**CAGACATCTGACGTCAGAGATA) were annealed, 5′-end-labeled with ^{32}P-ATP, and gel-purified on a 10% polyacrylamide 1× Tris-borate gel. *Boldface* represents SF1 binding site. Gels were exposed to film and the labeled oligonucleotides excised, eluted with fresh 0.5 M ammonium acetate buffer containing 1 mM EDTA, and precipitated with ethanol. Bacterially produced wild-type and mutant SF1 DBD proteins were each mixed with 15,000 cpm DNA probe and incubated for 10 min at room temperature in gel shift buffer [10 mM Tris (pH 7.7), 1 mM $MgCl_2$, 1 mM DTT, and 2 μg poly(deoxyinosine:deoxycytosine)]. Protein concentrations were measured spectrophotometrically (59). The solubility profile of each protein was monitored over the course of several days both spectrophotometrically as well as by running SDS-PAGE gels and visualizing the bands with Coomassie staining. The reactions were separated on a 5% polyacrylamide 1× Tris-borate gel, dried, and exposed to autoradiographic film and/or exposed to a phosphoscreen.

Coordinates

The atomic coordinates for the ensemble of NMR structures of the SF1 DBD-SBS DNA complex have been deposited with the RCSB PDB (code: 2FF0).

Acknowledgments

We thank Cynthia Daniels and Jayeeta Dhar for conducting some of the early work on this project and members of the Mayo and Radhakrishnan labs for useful discussions.

Received September 19, 2005. Accepted November 28, 2005.

Address all correspondence and requests for reprints to: Ishwar Radhakrishnan, Department of Biochemistry, Molecular Biology, and Cell Biology, Northwestern University, Evanston, Illinois 60208-3500. E-mail: i-radhakrishnan@northwestern.edu.

This work was supported by funds from the National Institutes of Health (NIH) Specialized Cooperative Centers Program in Reproductive Research (U54 HD41857) to K.E.M and I.R. C.M. is supported by an NIH Reproductive Biology training grant (T32 HD007068). I.R. is a Scholar of the Leukemia and Lymphoma Society. Z.Z. was supported by an undergraduate research grant from Northwestern University. We are grateful to the Robert H. Lurie Comprehensive Cancer Center for supporting structural biology research at Northwestern and the Keck Biophysics Facility for access to instrumentation.

Disclosure of Potential Conflicts of Interest: K.E.M. has consulted for World Book Science Inc., has equity interests in Ligand Pharmaceuticals Inc., and received lecture fees from Serono Inc., but has no conflicts with entities directly related to the material being published. All other authors have nothing to disclose.

REFERENCES

1. Perissi V, Rosenfeld MG 2005 Controlling nuclear receptors: the circular logic of cofactor cycles. Nat Rev Mol Cell Biol 6:542–554
2. McEwan IJ, ed. 2004 The nuclear receptor superfamily. London: Portland Press
3. Kumar R, Johnson BH, Thompson EB 2004 Overview of the structural basis for transcription regulation by nuclear hormone receptors. Essays Biochem 40:27–39
4. Val P, Lefrancois-Martinez AM, Veyssiere G, Martinez A 2003 SF-1 a key player in the development and differentiation of steroidogenic tissues. Nucl Recept 1:1–8
5. Parker KL, Rice DA, Lala DS, Ikeda Y, Luo X, Wong M, Bakke M, Zhao L, Frigeri C, Hanley NA, Stallings N, Schimmer BP 2002 Steroidogenic factor 1: an essential mediator of endocrine development. Recent Prog Horm Res 57:19–36
6. Lavorgna G, Ueda H, Clos J, Wu C 1991 FTZ-F1, a steroid hormone receptor-like protein implicated in the activation of fushi tarazu. Science 252:848–851
7. Honda S, Morohashi K, Nomura M, Takeya H, Kitajima M, Omura T 1993 Ad4BP regulating steroidogenic P-450 gene is a member of steroid hormone receptor superfamily. J Biol Chem 268:7494–7502
8. Luo X, Ikeda Y, Parker KL 1994 A cell-specific nuclear receptor is essential for adrenal and gonadal development and sexual differentiation. Cell 77:481–490
9. Sadovsky Y, Crawford PA, Woodson KG, Polish JA, Clements MA, Tourtellotte LM, Simburger K, Milbrandt J 1995 Mice deficient in the orphan receptor steroidogenic factor 1 lack adrenal glands and gonads but express P450 side-chain-cleavage enzyme in the placenta and have normal embryonic serum levels of corticosteroids. Proc Natl Acad Sci USA 92:10939–10943
10. Fayard E, Auwerx J, Schoonjans K 2004 LRH-1: an orphan nuclear receptor involved in development, metabolism and steroidogenesis. Trends Cell Biol 14:250–260
11. Gu P, Goodwin B, Chung AC, Xu X, Wheeler DA, Price RR, Galardi C, Peng L, Latour AM, Koller BH, Gossen J, Kliewer SA, Cooney AJ 2005 Orphan nuclear receptor LRH-1 is required to maintain Oct4 expression at the epiblast stage of embryonic development. Mol Cell Biol 25:3492–3505
12. Wang W, Zhang C, Marimuthu A, Krupka HI, Tabrizizad M, Shelloe R, Mehra U, Eng K, Nguyen H, Settachatgul C, Powell B, Milburn MV, West BL 2005 The crystal structures of human steroidogenic factor-1 and liver receptor homologue-1. Proc Natl Acad Sci USA 102:7505–7510
13. Li Y, Choi M, Cavey G, Daugherty J, Suino K, Kovach A, Bingham NC, Kliewer SA, Xu HE 2005 Crystallographic identification and functional characterization of phospholipids as ligands for the orphan nuclear receptor steroidogenic factor-1. Mol Cell 17:491–502
14. Krylova IN, Sablin EP, Moore J, Xu RX, Waitt GM, MacKay JA, Juzumiene D, Bynum JM, Madauss K, Montana V, Lebedeva L, Suzawa M, Williams JD, Williams SP, Guy RK, Thornton JW, Fletterick RJ, Willson TM, Ingraham HA 2005 Structural analyses reveal phosphatidyl inositols as ligands for the NR5 orphan receptors SF-1 and LRH-1. Cell 120:343–355
15. Ortlund EA, Lee Y, Solomon IH, Hager JM, Safi R, Choi Y, Guan Z, Tripathy A, Raetz CR, McDonnell DP, Moore DD, Redinbo MR 2005 Modulation of human nuclear receptor LRH-1 activity by phospholipids and SHP. Nat Struct Mol Biol 12:357–363
16. Luisi BF, Xu WX, Otwinowski Z, Freedman LP, Yamamoto KR, Sigler PB 1991 Crystallographic analysis of the interaction of the glucocorticoid receptor with DNA. Nature 352:497–505
17. Schwabe JW, Chapman L, Finch JT, Rhodes D 1993 The crystal structure of the estrogen receptor DNA-binding domain bound to DNA: how receptors discriminate between their response elements. Cell 75:567–578
18. Rastinejad F, Perlmann T, Evans RM, Sigler PB 1995 Structural determinants of nuclear receptor assembly on DNA direct repeats. Nature 375:203–211
19. Zhao Q, Khorasanizadeh S, Miyoshi Y, Lazar MA, Rastinejad F 1998 Structural elements of an orphan nuclear receptor-DNA complex. Mol Cell 1:849–861
20. Meinke G, Sigler PB 1999 DNA-binding mechanism of the monomeric orphan nuclear receptor NGFI-B. Nat Struct Biol 6:471–477
21. Zhao Q, Chasse SA, Devarakonda S, Sierk ML, Ahvazi B, Rastinejad F 2000 Structural basis of RXR-DNA interactions. J Mol Biol 296:509–520
22. Rastinejad F, Wagner T, Zhao Q, Khorasanizadeh S 2000 Structure of the RXR-RAR DNA-binding complex on the retinoic acid response element DR1. EMBO J 19: 1045–1054
23. Shaffer PL, Gewirth DT 2002 Structural basis of VDR-DNA interactions on direct repeat response elements. EMBO J 21:2242–2252
24. Devarakonda S, Harp JM, Kim Y, Ozyhar A, Rastinejad F 2003 Structure of the heterodimeric ecdysone receptor DNA-binding complex. EMBO J 22:5827–5840
25. Gearhart MD, Holmbeck SM, Evans RM, Dyson HJ, Wright PE 2003 Monomeric complex of human orphan estrogen related receptor-2 with DNA: a pseudo-dimer interface mediates extended half-site recognition. J Mol Biol 327:819–832
26. Shaffer PL, Jivan A, Dollins DE, Claessens F, Gewirth DT 2004 Structural basis of androgen receptor binding to selective androgen response elements. Proc Natl Acad Sci USA 101:4758–4763

27. Ueda H, Sun GC, Murata T, Hirose S 1992 A novel DNA-binding motif abuts the zinc finger domain of insect nuclear hormone receptor FTZ-F1 and mouse embryonal long terminal repeat-binding protein. Mol Cell Biol 12: 5667–5672
28. Wilson TE, Mouw AR, Weaver CA, Milbrandt J, Parker KL 1993 The orphan nuclear receptor NGFI-B regulates expression of the gene encoding steroid 21-hydroxylase. Mol Cell Biol 13:861–868
29. Ueda H, Hirose S 1991 Defining the sequence recognized with BmFTZ-F1, a sequence specific DNA binding factor in the silkworm, *Bombyx mori*, as revealed by direct sequencing of bound oligonucleotides and gel mobility shift competition analysis. Nucleic Acids Res 19: 3689–3693
30. Ito M, Park Y, Weck J, Mayo KE, Jameson JL 2000 Synergistic activation of the inhibin α-promoter by steroidogenic factor-1 and cyclic adenosine 3′,5′-monophosphate. Mol Endocrinol 14:66–81
31. Mukherjee A, Mayo KE 2001 Regulation of inhibin subunit gene expression by gonadotropins and cAMP in ovarian granulosa cells. In: Shupnik MA, ed. Gene engineering and molecular models of endocrinology. Totowa, NJ: Humana Press; 277–306
32. Li FQ, Ueda H, Hirose S 1994 Mediators of activation of fushi tarazu gene transcription by BmFTZ-F1. Mol Cell Biol 14:3013–3021
33. Takemaru K, Li FQ, Ueda H, Hirose S 1997 Multiprotein bridging factor 1 (MBF1) is an evolutionarily conserved transcriptional coactivator that connects a regulatory factor and TATA element-binding protein. Proc Natl Acad Sci USA 94:7251–7256
34. Kabe Y, Goto M, Shima D, Imai T, Wada T, Morohashi K, Shirakawa M, Hirose S, Handa H 1999 The role of human MBF1 as a transcriptional coactivator. J Biol Chem 274: 34196–34202
35. Brendel C, Gelman L, Auwerx J 2002 Multiprotein bridging factor-1 (MBF-1) is a cofactor for nuclear receptors that regulate lipid metabolism. Mol Endocrinol 16: 1367–1377
36. Solomon IH, Hager JM, Safi R, McDonnell DP, Redinbo MR, Ortlund EA 2005 Crystal structure of the human LRH-1 DBD-DNA complex reveals Ftz-F1 domain positioning is required for receptor activity. J Mol Biol 354:1091–1102
37. Stols L, Gu M, Dieckman L, Raffen R, Collart FR, Donnelly MI 2002 A new vector for high-throughput, ligation-independent cloning encoding a tobacco etch virus protease cleavage site. Protein Exp Purif 25:8–15
38. Radhakrishnan I, Perez-Alvarado GC, Parker D, Dyson HJ, Montminy MR, Wright PE 1999 Structural analyses of CREB-CBP transcriptional activator-coactivator complexes by NMR spectroscopy: implications for mapping the boundaries of structural domains. J Mol Biol 287: 859–865
39. Bax A, Grzesiek S 1993 Methodological advances in protein NMR. Accounts Chem Res 26:131–138
40. Ferentz AE, Wagner G 2000 NMR spectroscopy: a multifaceted approach to macromolecular structure. Q Rev Biophys 33:29–65
41. Yamazaki T, Forman-Kay JD, Kay LE 1993 2-Dimensional NMR experiments for correlating $^{13}C^{\beta}$ and $^{1}H^{\delta/\epsilon}$ chemical-shifts of aromatic residues in ^{13}C-labeled proteins via scalar couplings. J Am Chem Soc 115:11054–11055
42. Otting G, Wüthrich K 1990 Heteronuclear filters in two-dimensional [^{1}H,^{1}H]-NMR spectroscopy: combined use with isotope labelling for studies of macromolecular conformation and intermolecular interactions. Q Rev Biophys 23:39–96
43. Linge JP, Habeck M, Rieping W, Nilges M 2003 ARIA: automated NOE assignment and NMR structure calculation. Bioinformatics 19:315–316
44. Brünger AT, Adams PD, Clore GM, DeLano WL, Gros P, Grosse-Kunstleve RW, Jiang JS, Kuszewski J, Nilges M, Pannu NS, Read RJ, Rice LM, Simonson T, Warren GL 1998 Crystallography, NMR system: a new software suite for macromolecular structure determination. Acta Crystallogr D Biol Crystallogr 54:905–921
45. Zwahlen C, Legault P, Vincent SJF, Greenblatt J, Konrat R, Kay LE 1997 Methods for measurement of intermolecular NOEs by multinuclear NMR spectroscopy: application to a bacteriophage λ N-peptide/boxB RNA complex. J Am Chem Soc 119:6711–6721
46. Cornilescu G, Delaglio F, Bax A 1999 Protein backbone angle restraints from searching a database for chemical shift and sequence homology. J Biomol NMR 13:289–302
47. Saenger W 1988 Principles of nucleic acid structure. New York: Springer-Verlag
48. Laskowski RA, Rullmannn JA, MacArthur MW, Kaptein R, Thornton JM 1996 AQUA and PROCHECK-NMR: programs for checking the quality of protein structures solved by NMR. J Biomol NMR 8:477–486
49. Salerno WJ, Seaver SM, Armstrong BR, Radhakrishnan I 2004 MONSTER: inferring non-covalent interactions in macromolecular structures from atomic coordinate data. Nucleic Acids Res 32:W566–W568
50. Hutchinson EG, Thornton JM 1996 PROMOTIF—a program to identify and analyze structural motifs in proteins. Protein Sci 5:212–220
51. Pettersen EF, Goddard TD, Huang CC, Couch GS, Greenblatt DM, Meng EC, Ferrin TE 2004 UCSF Chimera—a visualization system for exploratory research and analysis. J Comput Chem 25:1605–1612
52. Nicholls A, Sharp KA, Honig B 1991 Protein folding and association: insights from the interfacial and thermodynamic properties of hydrocarbons. Proteins 11:281–296
53. Briers TW, van de Voorde A, Vanderstichele H 1993 Characterization of immortalized mouse granulosa cell lines. In Vitro Cell Dev Biol Anim 29A:847–854
54. Vanderstichele H, Delaey B, de Winter J, de Jong F, Rombauts L, Verhoeven G, Dello C, van de Voorde A, Briers T 1994 Secretion of steroids, growth factors, and cytokines by immortalized mouse granulosa cell lines. Biol Reprod 50:1190–202
55. Felgner PL, Gadek TR, Holm M, Roman R, Chan HW, Wenz M, Northrop JP, Ringold GM, Danielsen M 1987 Lipofection: a highly efficient, lipid-mediated DNA-transfection procedure. Proc Natl Acad Sci USA 84:7413–7417
56. Campbell MJ 1995 Lipofection reagents prepared by a simple ethanol injection technique. Biotechniques 18: 1027–1032
57. de Wet JR, Wood KV, DeLuca M, Helinski DR, Subramani S 1987 Firefly luciferase gene: structure and expression in mammalian cells. Mol Cell Biol 7:725–737
58. Fuerst TR, Earl PL, Moss B 1987 Use of a hybrid vaccinia virus-T7 RNA polymerase system for expression of target genes. Mol Cell Biol 7:2538–2544
59. Gill SC, von Hippel PH 1989 Calculation of protein extinction coefficients from amino acid sequence data. Anal Biochem 182:319–326

***Molecular Endocrinology* is published monthly by The Endocrine Society (http://www.endo-society.org), the foremost professional society serving the endocrine community.**